HHS Public Access

Author manuscript

J Thromb Haemost. Author manuscript; available in PMC 2023 February 01.

Published in final edited form as:

J Thromb Haemost. 2022 February ; 20(2): 486–497. doi:10.1111/jth.15617.

Breaking the fibrinolytic speed limit with microwheel co-delivery of tissue plasminogen activator and plasminogen

Dante Disharoon[†], **Brian G. Trewyn**[‡], **Paco S. Herson**[§], **David W.M. Marr**[†], **Keith B. Neeves**[¶]

[†]Department of Chemical and Biological Engineering, Colorado School of Mines, Golden, CO 80401, United States

[‡]Department of Chemistry, Colorado School of Mines, Golden, CO 80401, United States

[§]Department of Anesthesiology, University of Colorado Denver | Anschutz Medical Campus, Aurora, CO, 80045, United States

[¶]Departments of Bioengineering and Pediatrics, Hemophilia and Thrombosis Center, University of Colorado Denver | Anschutz Medical Campus, Aurora, CO 80045, United States

Abstract

Background: To reestablish blood flow in vessels occluded by clots, tissue plasminogen activator (tPA) can be used; however, its efficacy is limited by transport to and into a clot and by the depletion of its substrate, plasminogen.

Objectives: To overcome these rate limitations, a platform was designed to co-deliver tPA and plasminogen based on microwheels (μwheels), wheel-like assemblies of superparamagnetic colloidal beads that roll along surfaces at high speeds.

Methods: The biochemical speed limit was determined by measuring fibrinolysis of plasma clots at varying concentrations of tPA (10-800 nM) and plasminogen (1-6 μM). Biotinylated magnetic mesoporous silica nanoparticles were synthesized and bound to streptavidin coated superparamagnetic beads to make studded beads. Studded beads were loaded with plasminogen tPA was immobilized on their surface. Plasminogen release and tPA activity were measured on the studded beads. Studded beads were assembled into μwheels with rotating magnetic fields and fibrinolysis of plasma clots was measured in a microfluidic device.

Results: The biochemical speed limit for plasma clots was ~15 μm/min. Plasminogen loaded, tPA immobilized μwheels lyse plasma clots at rate comparable biochemical speed limit. With the

Correspondence: Keith B. Neeves, Ph.D., Departments of Bioengineering and Pediatrics, University of Colorado Denver | Anschutz Medical Campus, 12800 E. 19th St., Aurora, CO 80045, keith.neeves@cuanschutz.edu; David W.M. Marr, Ph.D, Department of Chemical and Biological Engineering, Colorado School of Mines, 1632 Illinois St., Golden, CO 80401, dmarr@mines.edu.

Author contributions:

Conceptualization: D. Disharoon, D. W. M. Marr, K. B. Neeves
Methodology: D. Disharoon, B. G. Trewyn, D. W. M. Marr, K. B. Neeves
Investigation: D. Disharoon
Supervision: D. W. M. Marr, K. B. Neeves
Writing: D. Disharoon, D. W. M. Marr, K. B. Neeves
Review and editing: D. Disharoon, D. W. M. Marr, K. B. Neeves, P. S. Herson, B. G. Trewyn

Conflict of Interest Declaration:

D.W.M.M. and K.B.N. own a patent that describes methods of forming and using μwheels (U.S. patent 10722250). The other authors declare that they have no competing interests.

addition of corkscrew motion, μwheels penetrate into clots, thereby exceeding the biochemical speed limit (~20 μm/min) and achieving lysis rates 40-fold higher than 50 nM tPA.

Conclusions: Co-delivery of an immobilized enzyme and its substrate via a microbot capable of mechanical work has the potential to target and rapidly lyse clots that are inaccessible by mechanical thrombectomy devices or recalcitrant to systemic tPA delivery.

Keywords

Colloids; fibrin; fibrinolysis; plasminogen; tissue plasminogen activator

Introduction

Fibrinolysis using tissue plasminogen activator (tPA) can reestablish blood flow in various types of thrombosis including myocardial infarction (1,2), deep vein thrombosis (3,4), pulmonary embolism (5,6), ischemic stroke (7,8), and limb ischemia (9). tPA works by binding to and converting the zymogen plasminogen to the enzyme plasmin, an interaction that is accelerated by two orders-of-magnitude in the presence of its co-factor fibrin (10). Plasmin in turn cleaves lysyl and arginyl bonds at many different sites to transect cross-linked fibrin fibers producing several different fragments (11).

The rate of fibrinolysis by tPA is limited by both transport processes and biochemical reactions (12). The transport of tPA to the clot periphery can be the rate limiting step in intravenous delivery because it is diffusion-dominated in occluded vessels with low or no blood flow (Fig. 1A) (13,14). Recombinant tPA (alteplase) has a half-life of minutes in blood due primarily to rapid receptor-mediated endocytosis in the liver and thus is often eliminated before it reaches a thrombus (15-17). These limitations can be partially overcome by catheter directed intraarterial delivery, however only 20% of stroke patients have large artery occlusions that are accessible to catheters (18). Tenecteplase is an engineered tPA that is less susceptible to endogenous inhibitors and has a higher specificity for fibrin (19-21), but it has not shown superior performance to alteplase in clinical trials for ischemic stroke (22). Even once delivered, penetration of tPA is limited by its high binding affinity (Kd = 0.6 μM (23)) to fibrin fibers which localizes it to the first few micrometers of the thrombus interface (24,25). Acting as an effective affinity filter, this leads to surface erosion with little penetration of tPA into the clot. While a direct strategy of increasing tPA concentration to overcome slow diffusion rates would seem desirable, this is bounded by the bleeding risks associated with degradation of fibrinogen, lysis of hemostatic clots, and tPA neurotoxicity (26,27).

Counterintuitively, the speed of fibrinolysis does not increase monotonically with tPA concentration. Rather, a bell-shaped curve has been reported with a maximum lysis rate occurring at ~20 nM tPA for compacted plasma clots (28). This is surprising because the plasma concentration of plasminogen (~2 μM) is much higher than the therapeutic tPA concentration (5-50 nM), an observation explained by consumption of local plasminogen due its high affinity (Kd = 0.25 μM (23)) binding to partially degraded fibrin and subsequent conversion to plasmin (29-32). Supplemental plasminogen and platelet-bound plasminogen

enhance the fibrinolysis rates (33,34) suggesting that plasminogen is the limiting factor in the presence of high plasminogen activator concentrations (Fig. 1B).

The functionalization of micro- and nanoparticles with tPA overcomes some of the transport and kinetic limitations of fibrinolysis by protecting tPA from inhibition by PAI-1 and PAI-2, and using targeting moieties to platelet glycoprotein 1b alpha (GP1bα), activated $\alpha_{IIb}\beta_3$ integrins, or fibrin that localize particles on a clot while maintaining low circulating concentrations (35). Microparticles manipulated by external fields, or microbots, offer further advantages of not relying on blood flow for delivery (36,37). For example, tPA functionalized magnetic particles pulled towards a clot with a magnetic field gradient improves thrombolytic outcomes in mouse (38) and rat (39-41) models of thrombosis compared to free tPA. Rotating magnetic microbots can also act as local mixers, reducing concentration gradients near the interface of a clot to accelerate tPA-mediated thrombolysis (37).

Microbots are promising therapeutic vehicles because of their potential to target drug delivery to disease-afflicted sites within the body (42). Their propulsion can be achieved using applied magnetic (43,44), electric (45), optic (46), and acoustic fields (47,48). Of these strategies, magnetic field-based propulsion approaches are particularly well suited for in vivo applications because magnetic fields do not attenuate in tissue (49) and are not harmful to the human body. As a result, magnetically-controlled microbots have been proposed for the treatment of cancer (50,51), ocular surgery (52), and tissue damage (53) where targeted drug delivery could provide substantial benefit.

Building on these studies, we have shown that microbots can not only deliver drug but also impart mechanical action to aid in drug efficacy, specifically in the targeting of blood clots for the treatment of stroke (54). In previous work with assemblies of superparamagnetic microparticles functionalized with tPA (tPA-μwheels), we have shown that actuation using rotating magnetic fields enables both delivery at high concentrations and mechanical disruption of clots, ultimately leading to an inside-out bulk erosion (Fig. 1C) (54). However, while we were able to achieve local tPA concentrations that were three orders-of-magnitude higher than those reached by diffusive delivery of tPA, this resulted in only a one order-of-magnitude increase in fibrinolysis speed. Based on these results it appears that fibrinolysis using tPA-μwheels is plasminogen limited as reported in other studies of fibrinolysis at high tPA concentrations (54). To overcome this limitation and further enhance lysis speed, we develop here a μwheel-based strategy of delivering both tPA and plasminogen using tPA-μwheels coupled with mesoporous silica nanoparticles (MSN), which can provide controlled release of proteins (55-57). These co-laden μwheels break the biochemical speed limit by supplementing fresh plasminogen and burrowing their way into plasma clots (Fig. 1D).

Materials and Methods

Materials

10 nm (II,III) iron oxide nanoparticles (CAS 900084), cetyltrimethylammonium bromide (CTAB, CAS 57-09-0), sodium dodecyl sulfate (SDS, CAS 151-21-3), sodium borohydride (NaBH4, CAS 16940-66-2), bovine serum albumin (BSA, CAS 9048-46-A), fibrinogen

from human plasma (CAS 9001-32-5), human plasminogen (SRP6518), and plasmin activity assay kit (MAK244) were purchased from Sigma-Aldrich (St. Louis, MO). Ethyl acetate (142-89-2), ammonium hydroxide (1336-21-6) were obtained from Spectrum (New Brunswick, NJ). Zeba desalting columns (89882), EZ-LinkTM Sulfo-NHS-Biotin kits (A39256), Dynabeads™ MyOne™ Streptavidin T1 (beads, 65601), tetraethyl orthosilicate (TEOS, O46174), and Alexa 555 (A20174) were obtained from Thermo Fisher Scientific (Waltham, MA). Normal pooled plasma (NPP) was purchased from George King Bio-Medical, Inc. (Overland Park, KS). Human alpha thrombin was obtained through Enzyme Research Laboratories (South Bend, IN). Recombinant human tPA was purchased from Abcam (Cambridge, UK).

Synthesis of magnetic mesoporous silica nanoparticles (mMSN)

Synthesis of mMSN was adapted from Suteewong et al. (58) where 15 mg of 10 nm iron oxide nanoparticles in chloroform were passivated in 54.8 mM CTAB via 5 min homogenization. The resulting emulsion was heated to 70°C for 10 min to evaporate the chloroform before being diluted 20X in 18.2 MΩ-cm DI water. Ethyl acetate, ammonium hydroxide, and TEOS at 0.062 M, 0.46 M and 0.015 M respectively were allowed to react for 8 min before being neutralized using 2 M hydrochloric acid (HCl). The resulting particles were calcinated at 500 °C for 8 hr to remove the surfactant template before being resuspended in DI water with 0.1 wt% SDS. The entire reaction was carried out in a directional, no-gradient 4 mT magnetic field to bias the orientation of the iron oxide domains and maximize magnetic response. For some samples, mMSN were etched with NaBH4 for 4 hr to increase pore diameter after neutralization.

Characterization of mMSN

Scanning transmission electron microscopy (STEM) images were captured using a Talos F200X microscope at an accelerating voltage of 200 keV. High-angle annular dark field energy-dispersive X-ray (HAADF-EDS) spectra were also generated. Exposure times were greater than 30 min to allow for estimation of sample composition within a 90% confidence interval. Pore size distribution was measured using a Micromeritics Tristar 3000 sorptometer and calculated using the Barrett-Joyner-Halenda (BJH) method (59). Magnetization was characterized in an MPMS3 Quantum Design magnetometer at 25 °C from −0.5 to 0.5 T.

Loading and release of plasminogen

mMSN (10^6/μL) were incubated in a 0.5 mL solution containing 10 μM plasminogen in PBS for 24 hr. Immediately before use, the pgn-mMSN were removed from solution via centrifugation at 5000g for 5 min, washed three times in 0.5 mL phosphate-buffered saline (PBS), and resuspended in either PBS with 0.1 wt% SDS or plasma with 1 wt% BSA. A standard curve for plasminogen absorbance at 285 nm (A285) in PBS (0-20 μM) was measured with a UV-Vis spectrophotometer (Genesys 10S, ThermoFisher). Pgn-mMSN (10^5/μL) were placed in 0.5 mL PBS. To estimate maximum release, pgn-mMSN were allowed to incubate in PBS for 24 hr before being removed via centrifugation. Maximum plasminogen release was calculated from the A285 and standard curve data. To probe the release profile of pgn-mMSN over one hour, samples were centrifuged and the supernatants collected into cuvettes every 5 min. Once the A285 was measured, the supernatant was used

to resuspend the pgn-mMSN. A285 measurements were compared against a standard curve to calculate the release of plasminogen over time.

Biotinylation of tPA

Recombinant tPA at 200 ug/mL was biotinylated with an EZ-Link Sulfo-NHS-Biotin kit and purified in Zeba Spin Desalting Columns according to manufacturer instructions. To prepare tPA functionalized beads (tPA-beads), 5 μL beads were incubated in 20 μL aliquots of 200 μg/mL biotinylated tPA at 4 °C for 12 hr (tPA-beads). Excess tPA was removed with four washes via centrifugation at 1500 g for 1 minute. tPA-beads were resuspended in TBS with 1 wt% BSA.

Co-functionalization of beads with tPA and pgn-mMSN

To functionalize mMSN with primary amines, mMSN were incubated in 0.04 M 3-aminopropyltriethoxysilane (APS) in ethanol for 2 hr at room temperature, and then 1 hr at 80 °C (60). The mMSN were then washed with ethanol 4 times via centrifugation at 1500g for 1 min and finally resuspended in a 1:1 mixture of water and dimethyl sulfoxide (DMSO) (pH = 4.7). Then mMSN at $10^{14}/\mu L$ were mixed with 2 mL of 0.06M biotin in DMSO under sonication for 2 hr at room temperature. The resulting solution was washed 4 times with Tris-buffer solution (TBS, pH = 7.4) via centrifugation at 1500g for 1 min. After the final wash cycle, the biotinylated mMSN were resuspended with $10^{7}/\mu L$ beads in TBS for 4-48 hr. A magnet was used to separate the beads from the unbound mMSN in four separate washing cycles. Each time, beads with covalently attached mMSN (studded beads) were resuspended in TBS. Biotinylated tPA (200 μg/mL) was added to the solution and the studded beads allowed to incubate for 12 hr at 2 °C before four more wash cycles. Finally, the studded beads were incubated in 10 μM plasminogen in TBS for 12 hr at 4°C. Immediately before use, the resulting beads co-functionalized with tPA and pgn-mMSN (pgn-tPA-beads) were washed three times in TBS to remove excess plasminogen.

Plasmin Activity Assays

A fluorometric activity assay was used to measure plasmin activity on μwheels after plasminogen loading. Plasmin activity was measured according to manufacturer's instructions (MAK244, Sigma-Aldrich). The supernatant after the first wash step following the preparation of pgn-tPA-beads was diluted 10X and used to measure activation of plasminogen during studded tPA-bead incubation with plasminogen. To measure whether plasmin adsorbed to the tPA-bead surface, tPA-beads were mixed with 10 uM plasminogen in PBS for 24 hr, washed, then mixed with the plasmin assay buffer. To determine plasmin activation in a 60 min lysis experiment, pgn-tPA-beads were mixed with plasma for 60 min. Immediately before use, 12.5 μL of the fluorometric substrate (diluted 25X from the assay kit stock) was added to each sample. The beads were removed via centrifugation and the supernatant prepared with the fluorometric substrate. A microplate reader (Biotek Synergy H1, BioTek U.S. Winooski, VT) with λ_{ex} = 360 nm and λ_{em} = 450 nm measured relative fluorescent units (RFU) as a function of time.

Magnetic field induced assembly and translation

Under the influence of a rotating magnetic field, tPA-beads and pgn-mMSN spontaneously assemble into μwheels (54,61). To direct the μwheels to the fibrin front, a rotating AC magnetic field was generated using five air-cored solenoids (51 mm inner diameter) with 336 turns each. An analog output card (National Instruments (NI), NI-9623, Austin, TX) controlled by Matlab, generated a current that was subsequently amplified (Behringer, EP2000, Willich, Germany). The final current passing through each coil, measured using an analog input card (NI-USB-6009), was 2 A, resulting in a field strength of 6.2 mT at the sample. The frequency of the rotating field was 10 Hz. For corkscrew experiments, the heading direction and camber angle for each magnetic field were shifted over time such that the beads followed a forward-biased spiral path with a 1 sec frequency. μWheel velocity was tracked using brightfield microscopy on a Prior Open Stand microscope (Prior Scientific, Cambridge, UK) with a PCO Panda camera (PCO Imaging, Kelheim, Germany).

Measurement of tPA activity on functionalized beads

tPA (0.25, 0.5, 0.75 and 1 μM) and tPA-beads (10^5 and 10^6/μL) were incubated with excess (100 μM) fluorogenic substrate for tPA (SN-18, Haematologic Technologies Inc., Essex Junction, VT). For solvated tPA experiments, fluorescent intensity was measured in a microplate reader (Biotek Synergy H1, BioTek U.S. Winooski, VT) every minute for 1 hr. For tPA-bead experiments, the solution was rotated on a carousel to prevent bead settling. In 5 min intervals, beads were extracted from solution using a permanent magnet and the fluorescent intensity of the supernatant measured. Beads and supernatant were remixed after each measurement to ensure experimental continuity.

Fabrication of microfluidic devices

A template for the microfluidic channel was 3D printed using a Formlabs Form 3 printer using clear stereolithography resin (RS-F2-GPCL-04, Formlabs, Somerville, MA). The device has two inlets for the central channel (h = 50 μm) and two auxiliary inlets for the side chamber (h = 100 μm). A polydimethylsiloxane (PDMS) mold was made from the template. The PDMS was prepared using a 10:1 ratio of Sylgard 184 silicone elastomer base to curing agent (Dow Corning Corporation, Midland, MI). The mold was degassed for 1 hr in a vacuum chamber before being cured for 1 hr at 80 °C. Once cured, the mold was washed for 5 min in acetone and 5 min in ethanol in a sonicator before being air-dried. The mold and a glass slide were treated with oxygen plasma (0.2 torr) for 90 s and immediately bonded. The bonded assembly was annealed and then placed in a convection oven at 80 °C for 24 hr.

Fibrinolysis experiments

The geometry for the device is shown in Fig. S1. The two auxiliary inputs were plugged to prepare for injection of NPP, 30 μg/mL of Alexa 555 labeled fibrinogen, 20 mM $CaCl_2$ and 9 nM thrombin to form a fibrin gel in the right channel. The device was enclosed in a Petri dish for 30 min with a moist Kimwipe to prevent evaporation and to allow full gelation. Next, the auxiliary chamber was filled with NPP and a suspension of tPA-beads and pgn-mMSN was injected 1 mm from the fibrin front. Lysis experiments were recorded

using epifluorescence and brightfield microscopy through a PCO Panda camera at 5 min intervals through a 40X objective (NA 0.95, Plan APO). Because the fibrin front is not perfectly uniform, the front location was calculated as the average horizontal pixel over all vertical pixels in a captured frame.

Fibrinogen degradation product assays

Fibrinogen degradation product (FDP) was measured by ELISA according to the manufacturer's instructions (MBS2022486, MyBioSource, San Diego, CA). Absorbance at 450 nm was measured on the Biotek Synergy H1 plate reader. To measure fibrinogenolysis while beads were in suspension, tPA-beads, tPA beads and 4 μM plasminogen, and pgn-tPA-beads were incubated in NPP at room temperature for 1 hr and then centrifuged for 2 min at 1000g to isolate the supernatant. All tPA functionalized beads were at a concentration comparable to a tPA activity of 50 nM, NPP with no beads was used as a negative control and 2 μM plasmin was used as a positive control. To measure fibrinogenolysis during fibrinolysis experiments, a permanent magnet was used to move beads back and forth within the auxiliary channel (Fig. S1) ten times to induce mixing, and then to reconcentrate the beads at the fibrin front. Using two pipettes, 2 μL NPP was added to an auxiliary inlet at the same time as 2 μL was withdrawn from the auxiliary chamber. This sampling was repeated at 15 min intervals.

Statistical Analysis

Statistical significance for differences in fibrinolysis rates achieved using μwheel populations and soluble tPA (Fig 4C) was checked using one-way ANOVA with a 99% confidence threshold for statistical significance. Sample sizes were n = 5.

Results

Plasminogen depletion limits fibrinolysis rate at high tPA concentrations

To measure the extent to which fibrinolysis is rate-limited by tPA, we exposed a plasma clot formed with thrombin (9 nM) to varying concentrations of tPA and plasminogen (Fig. 2A). For a physiologic plasminogen concentration of 1 μM, the fibrinolysis rate, defined by the dissolution of the fibrin front over time, increases with increasing tPA concentrations from 50 nM up to 200 nM tPA (Fig. 2A, first column). However, at tPA concentrations > 200 nM the lysis rate decreases. Doubling the plasminogen concentration to 2 μM while holding tPA concentration at 50 nM resulted in a 65% increase in lysis rate and up to a 120% increase in lysis rate at tPA concentrations of 250-800 nM. Note that there is an optimal plasminogen concentration for a given tPA concentration that yields the maximum lysis rate (Fig. 2A,B). Plasminogen concentrations above this optimum attenuate fibrinolysis suggesting a competition for fibrin binding sites between tPA and plasminogen. Here, it is apparent that there is a biochemical speed limit of ~15.5 μm/min in the range to 200-600 nM tPA and 2-4 μM plasminogen, suggesting that a strategy of co-delivering tPA and plasminogen at these concentrations could significantly accelerate fibrinolysis. μWheels are well-suited for such a strategy because they are assembled from component, potentially-multifunctional, building blocks and can be driven to and accumulate at the edge of a clot,

achieving a high local concentration of both the enzyme and its substrate adjacent to their co-factor.

Synthesis and characterization of plasminogen releasing magnetic colloids

To create tPA-μwheels, we functionalize streptavidin Dynabeads™ (beads) with biotinylated tPA (tPA-beads) (Fig. 3A). These tPA-beads readily assemble into tPA-μwheels with application of a magnetic field (54). To co-deliver plasminogen and tPA, we use mesoporous silica nanoparticles (MSN) with incorporated iron oxide nanoparticles to make them magnetic and increase coupling rate of beads and MSN. We covalently coupled biotinylated magnetic MSN (mMSN) to beads to create studded beads, then functionalized the studded beads with tPA (tPA-studded beads) (Fig. 3A). Finally, the tPA-studded beads were incubated with plasminogen to load the mMSN to yield a superparamagnetic bead that can release plasminogen and carry immobilized tPA (pgn-tPA-beads) (Fig. 3A). When pgn-tPA-beads are subject to a rotating magnetic field, they assembly into wheel like structures we refer to as pgn-tPA-μwheels.

The mMSN were synthesized with an average diameter 161 ± 57 nm and circularity 0.61 ± 0.17 and imaged using transmission electron microscopy (TEM) (Fig. 3B). Iron oxide content was measured at 10.5 wt% with 90% confidence using quantitative energy dispersive X-ray spectroscopy (EDS) (Fig. 3C). Nitrogen sorption isotherms show adsorption at relative pressures between 0.3 and 1.0 with most hysteresis occurring at $\frac{P}{P_0} = 0.7$ (Fig. 3D), indicating the presence of both micro- and mesopores with a wide range of pore sizes. The Barrett-Joyner-Halenda (BJH) method was used to determine an accessible pore volume of 0.6 cm^3/g distributed over a wide range of pore sizes with an average of 14.6 ± 5.7 nm. Magnetization curves for the mMSN confirmed that the particles are paramagnetic and amenable to magnetic control (Fig. 3E) allowing us to couple them to superparamagnetic beads with long-range magnetic attractions more efficiently than by mixing alone. Coupling between mMSN and beads to make studded beads was verified using scanning electron microscopy (SEM) (Fig. 3F).

A strategy that relies solely on higher tPA concentrations does not necessarily lead to faster lysis (Fig. 2B). One of the features of the synthesis approach (Fig. 3A) is that the relative concentrations of tPA and plasminogen can be adjusted independently by varying the ratio of tPA-beads to plasminogen-loaded mMSN. To control the number of mMSN per bead, or coverage, we varied the mixing time of the streptavidin beads and biotinylated mMSN (Fig. 3G). The coverage is 0-2 after 3 hr and 3-5 after 48 hr, a relatively slow association rate likely limited by steric hindrance at the bead surface. To achieve higher coverage, a 4 mT uniform magnetic field was applied across the sample, roughly doubling the coverage ratio for all mixing times (Fig. 3G). This mixing time and magnetic field were used to synthesize studded beads for fibrinolysis experiments.

After conjugation to tPA, studded tPA-beads were loaded with plasminogen via incubation for 24 hr. Though we observed some plasmin activation during the loading step, pgn-tPA-beads had insignificant plasmin activity after washing (Fig S2). Plasminogen release kinetics from pgn-mMSN and pgn-tPA-beads were measured by UV absorbance (Fig. 3H). Pgn-

tPA-beads have a lower loading capacity than pgn-mMSN, likely because some pores are inaccessible when coupled to beads. The amount of plasminogen released from pgn-tPA-beads was 66 ± 2% of that released from pgn-mMSN for a fixed mMSN number density. The activity of tPA- and pgn-tPA-beads used for lysis experiments is equivalent to 8 nM tPA, a value not significantly affected by co-functionalization with pgn-mMSN (Fig. 3I).

A potential advantage of immobilizing tPA on bead surfaces is mitigated systemic fibrinogenolysis. We measured the FDP present in NPP after 60 min incubation with bead populations having an effective activity of 50 nM tPA (Fig 3J). While soluble-phase tPA caused a doubling of FDP present in NPP, tPA-beads caused no significant change. Pgn-tPA-beads and tPA-beads in the presence of 4 μM plasminogen caused 60% less fibrinogenolysis as compared to free tPA.

Fibrinolysis with μwheel co-delivery of tPA and plasminogen—Fibrinolysis experiments were conducted on plasma clots with five formulations: free tPA, tPA-beads, tPA-beads with 4 μM free plasminogen, tPA-beads and pgn-mMSN (uncoupled), and pgn-tPA-beads (coupled) (Fig. 4A, Video S1). Particles with an initial activity equivalent to 8 nM tPA or free tPA (50 nM) were injected 1 mm from the fibrin front and a rotating magnetic field (6.2 mT, 10 Hz) was used to roll magnetic particles and their μwheel assemblies to the fibrin gel front. Free tPA caused significant fibrinogenolysis (Fig. S3) and diffused slowly to the fibrin front, resulting in negligible fibrinolysis for the first 20 min of the experiment (Fig. 4B). Once measurable, lysis proceeded at a linear rate of 0.42 ± 0.13 μm/min for the duration of the experiment (Fig. 4B, C).

Experiments using tPA-beads were characterized by a shorter lag time for fibrinolysis (~10 min) than tPA as μwheels translate and accumulate at the fibrin front faster than diffusion (Fig. 4B). After this lag time, lysis rate accelerated as the accumulation of tPA-μwheels increased until it reached a maximum of 2.9 ± 0.7 μm/min (Fig. 4C) and then decreased after ~35 min as plasminogen became locally depleted. When tPA-μwheels were supplemented with 4 μM plasminogen, lysis rates accelerated significantly, reaching 14.4 ± 3.9 μm/min, close to the biochemical speed limit described in Fig. 1. Uncoupled pgn-mMSN with tPA-wheels failed to recapitulate the benefits of supplemental plasminogen with the maximum lysis rate reaching 4.5 ± 1.2 μm/min (Fig. 4C). This relatively modest increase compared to tPA-beads alone is due to a limited amount of plasminogen replenishment.

The lysis rate of pgn-tPA-μwheels reaches a maximum rate of 13.6 ± 0.9 μm/min (Fig. 4C) for the first 30 min of the experiment (Fig. 4B), consistent with the measured plasminogen release kinetics (Fig. 3H). FDP generation for both tPA-uwheels and pgn-tPA-uwheels was below the detection limit during lysis experiments (Fig. S3). The lag time is reduced for pgn-tPA-μwheels because of their increased average translation speed relative to tPA-μwheels (Fig. S4A-B). After 30 min, the pgn-tPA-μwheel lysis rate approaches the rate of tPA-μwheels since most plasminogen has been released. Notably, this formulation reaches the biochemical speed limit of ~15.5 μm/min (Fig. 2B) suggesting that both tPA and plasminogen are near their target concentrations.

In order to break the biochemical speed limit, we used the magnetic field to manipulate μwheels along a corkscrew trajectory as we have previously demonstrated that this allows μwheels to penetrate into clots (54). Pgn-tPA-μwheels following a corkscrew trajectory (Video S2) are 40-fold more effective fibrinolytics than 50 nM tPA and reach a maximum lysis rate of 20.3 ± 1.0 μm/min (Fig. 4B). As μwheels burrow their way into a clot (Video S3), new fibrin fibers are available for binding of tPA and plasmin(ogen) that are not accessible during surface erosion. This mechanical penetration combined with high tPA and plasminogen concentration yields an inside-out lysis pattern that exceeds the maximum lysis rate achieved using only biochemical means.

Discussion

The speed of fibrinolysis is governed by a series of rate-limiting transport and biochemical reaction steps. We have attempted to overcome each of those steps with the co-delivery of a fibrinolytic enzyme, tPA, and its substrate, plasminogen, with a magnetically powered microbot. We measured the biochemical speed limit of fibrinolysis using different combinations of tPA and plasminogen concentrations and found that we can break that limit using this co-delivery strategy in combination with mechanical action created through corkscrew motion of μwheels.

The first rate-limiting step that must be overcome to achieve thrombolysis is the transport of fibrinolytics like tPA to a clot. Systemic delivery of fibrinolytic agents relies on diffusion to reach an impermeable occlusive clot (13), which is slow compared to active modes of transport or convection. We overcome this transport barrier by immobilizing tPA on magnetic beads which are assembled into μwheels that roll along a straight path to the clot. Using the active transport reduced the lag time to the start of fibrinolysis. Active transport also provides the opportunity to have a subtherapeutic circulating concentration of tPA immobilized on beads that accumulates at the clot at very high concentration.

The second rate-limiting step is the binding of tPA to fibrin. This step can be accelerated by increasing the concentration of tPA in systemic or intraarterial delivery. However, this approach is limited by the bleeding risk associated with high systemic concentrations of tPA. Using a μwheel delivery strategy offers an alternative solution because μwheels can be injected at subtherapeutic systemic concentration of tPA and subsequently localize at high concentrations at the clot interface. For example in this study, our pgn-tPA-beads with an activity comparable to 8 nM of free tPA were injected 1 mm upstream of the clot in a manner reflective of catheter delivery. While the tPA activity of the accumulated μwheels at the clot interface is > 250 nM. tPA immobilized on microparticles is also less likely to enter the extravascular space due to their size and therefore has the potential to be less neurotoxic in stroke applications.

At sufficiently high tPA concentrations, plasminogen is the limiting factor in fibrinolysis speed (62). Once the fibrin front is replete with tPA, increasing tPA concentration further inhibits fibrinolysis because tPA both consumes the available plasminogen and competes with plasmin and plasminogen for fibrin binding sites. Here, we demonstrate that this

limitation can not only be overcome by co-delivering a plasminogen payload with tPA using a microbot platform but can also approach the biochemical speed limit.

Both tPA and plasminogen have high affinity for fibrin fibers which limits their penetration into a clot leading to surface erosion of a clot with minimal permeation. Thus, the last rate limiting step to overcome is the number of accessible fibrin binding sites (63). We have previously shown the potential to access binding sites within the interior of a clot, and a bulk erosion from the inside-out, using a μwheel corkscrew motion (54). We also showed that tPA-μwheels are capable of lysing platelet-rich clots formed from whole blood, demonstrating their use in more physiological conditions, though we did not consider the effects of other cellular matter such as histones and neutrophil extracellular traps in those studies. Here we show that the corkscrew motion, in combination with co-delivery of tPA and plasminogen, breaks the biochemical speed limit in plasma clots by allowing μwheels to penetrate into the clot.

Using magnetically actuated pgn-tPA-μwheels, we have overcome each rate limiting step and achieved lysis rates that exceed even supratherapeutic concentrations of tPA. Our 40-fold increase in lysis rate over therapeutic concentrations of 50 nM tPA is a larger relative increase compared to other approaches that use magnetic particles as adjuvants or drug delivery vehicles (35). For example, using magnetic microparticles to augment tPA penetration into clots approximately doubles thrombolysis rates (64), a rate that can be further enhanced with the addition of ultrasound. Magnetic rod mixers can enhance the mass transfer of tPA such that fibrinolysis at lower concentrations of tPA can approach, but not exceed, that of supratherapeutic concentrations (37). However, strategies that increase the accessibility of local tPA ultimately run up against the limit of plasminogen availability. Because our approach uses beads encapsulating iron oxide, further enhancement of fibrinolysis rate could be achieved using high frequency magnetic fields to induce local hyperthermia, which has been shown to accelerate fibrinolysis in vitro and in vivo using tPA-functionalized iron oxide nanocubes (38). Furthermore, we demonstrate that tPA-μwheels and pgn-tPA-μwheels cause less fibrinogenolysis than soluble-phase tPA, potentially mitigating some of the bleeding risk associated with fibrinolytic therapy. Taken together, the combination of multifunctional magnetic particles combined with dynamic magnetic fields has great potential to improve the rate of recanalization of occluded blood vessels, especially in cases like lacunar strokes where clots are not accessible to mechanical thrombectomy devices.

Supplementary Material

Refer to Web version on PubMed Central for supplementary material.

Acknowledgments:

The authors acknowledge support from the National Institutes of Health under grants R21AI138214 and R01NS102465. D.D. was supported by an American Heart Association Predoctoral Fellowship Award 18PRE34070076. Illustrations made with BioRender.com.

References

1. Krittanawong C, Hahn J, Kayani W, Jneid H. Fibrinolytic Therapy in Patients with Acute ST-elevation Myocardial Infarction. Vol. 10, Interventional Cardiology Clinics. Elsevier Inc.; 2021. p. 381–90. [PubMed: 34053624]
2. van de Werf F, Arnold AER. Intravenous tissue plasminogen activator and size of infarct, left ventricular function, and survival in acute myocardial infarction. British Medical Journal. 1988;297(6660):1374–9. [PubMed: 3146370]
3. Goldhaber SZ, Meyerovitz MF, Braunwald E, Green D, Vogelzang RL, Citrin P, Heit J, Sobel M, Brownell Wheeler H, Plante D, Kim H, Hopkins A, Tufte M, Stump D. Randomized controlled trial of tissue plasminogen activator in proximal deep venous thrombosis. The American Journal of Medicine. 1990;88(3):235–40. [PubMed: 2106783]
4. Fleck D, Albadawi H, Shamoun F, Knuttinen G, Naidu S, Oklu R. Catheter-directed thrombolysis of deep vein thrombosis: Literature review and practice considerations. Vol. 7, Cardiovascular Diagnosis and Therapy. AME Publishing Company; 2017. p. S228–37. [PubMed: 29399526]
5. Stewart LK, Kline JA. Fibrinolytics for the treatment of pulmonary embolism. Vol. 225, Translational Research. Mosby Inc.; 2020. p. 82–94. [PubMed: 32434005]
6. Levine M, Hirsh J, Weitz J, Cruickshank M, Neemeh J, Turpie AG, Gent M. A randomized trial of a single bolus dosage regimen of recombinant tissue plasminogen activator in patients with acute pulmonary embolism. Chest. 1990;98(6):1473–9. [PubMed: 2123152]
7. Sandercock P, Wardlaw JM, Lindley RI, Dennis M, Cohen G, Murray G, Innes K, Venables G, Czlonkowska A, Kobayashi A, Ricci S, Murray V, Berge E, Slot KB, Hankey GJ, Correia M, Peeters A, Matz K, Lyrer P, et al. The benefits and harms of intravenous thrombolysis with recombinant tissue plasminogen activator within 6 h of acute ischaemic stroke (the third international stroke trial [IST-3]): A randomised controlled trial. The Lancet [Internet]. 2012;379(9834):2352–63. Available from: 10.1016/S0140-6736(12)60768-5
8. Emberson J, Lees KR, Lyden P, Blackwell L, Albers G, Bluhmki E, Brott T, Cohen G, Davis S, Donnan G, Grotta J, Howard G, Kaste M, Koga M, von Kummer R, Lansberg M, Lindley RI, Murray G, Olivot JM, et al. Effect of treatment delay, age, and stroke severity on the effects of intravenous thrombolysis with alteplase for acute ischaemic stroke: A meta-analysis of individual patient data from randomised trials. The Lancet. 2014;384(9958):1929–35.
9. Byrne RM, Taha AG, Avgerinos E, Marone LK, Makaroun MS, Chaer RA. Contemporary outcomes of endovascular interventions for acute limb ischemia. Journal of Vascular Surgery [Internet]. 2014;59(4):988–95. Available from: 10.1016/j.jvs.2013.10.054 [PubMed: 24360240]
10. Hoylaerts M, Rijken DC, Lijnen HR, Collen D. Kinetics of the activation of plasminogen by human tissue plasminogen activator. Role of fibrin. Journal of Biological Chemistry [Internet]. 1982;257(6):2912–9. Available from: 10.1016/S0021-9258(19)81051-7
11. Francis CW, Marder VJ, Barlow GH. Plasmic degradation of crosslinked fibrin. Characterization of new macromolecular soluble complexes and a model of their structure. Journal of Clinical Investigation. 1980;66(5):1033–43.
12. Diamond SL. Engineering Design of Optimal Strategies for Blood Clot Dissolution. Annual Review of Biomedical Engineering [Internet]. 1999;1(1):427–61. Available from: http://www.annualreviews.org/doi/10.1146/annurev.bioeng.1.1.427
13. Labiche LA, Malkoff M, Alexandrov A v. Residual flow signals predict complete recanalization in stroke patients treated with TPA. Journal of Neuroimaging. 2003;13(1):28–33. [PubMed: 12593128]
14. Sabovic M, Blinc A. Biochemical and biophysical conditions for blood clot lysis. Pflugers Archiv European Journal of Physiology. 2000;440(SUPPL. 5):134–6.
15. Acheampong P, Ford GA. Pharmacokinetics of alteplase in the treatment of ischaemic stroke. Expert Opinion on Drug Metabolism and Toxicology. 2012 Feb;8(2):271–81. [PubMed: 22248305]
16. Chandler WL, Alessi MC, Aillaud MF, Henderson P, Vague P, Juhan-Vague I. Clearance of Tissue Plasminogen Activator (TPA) and TPA/Plasminogen Activator Inhibitor Type 1 (PAI-1) Complex. Circulation. 1997;96(3):761–8. [PubMed: 9264480]

17. von Kummer R Early Major Ischemic Changes on Computed Tomography Should Preclude Use of Tissue Plasminogen Activator. Stroke. 2003;34(3):820–1. [PubMed: 12624316]

18. Henderson SJ, Weitz JI, Kim PY. Fibrinolysis: strategies to enhance the treatment of acute ischemic stroke. Journal of Thrombosis and Haemostasis. 2018;16(10):1932–40. [PubMed: 29953716]

19. Tanswell P, Modi N, Combs D, Danays T. Pharmacokinetics and Pharmacodynamics of Tenecteplase in Fibrinolytic Therapy of Acute Myocardial Infarction.

20. Baruah DB, Dash RN, Chaudhari MR, Kadam SS. Plasminogen activators: A comparison. Vol. 44, Vascular Pharmacology. 2006. p. 1–9. [PubMed: 16275118]

21. Campbell BCV, Mitchell PJ, Churilov L, Yassi N, Kleinig TJ, Dowling RJ, Yan B, Bush SJ, Dewey HM, Thijs V, Scroop R, Simpson M, Brooks M, Asadi H, Wu TY, Shah DG, Wijeratne T, Ang T, Miteff F, et al. Tenecteplase versus Alteplase before Thrombectomy for Ischemic Stroke. New England Journal of Medicine. 2018;378(17):1573–82.

22. Logallo N, Novotny V, Assmus J, Kvistad CE, Alteheld L, Rønning OM, Thommessen B, Amthor KF, Ihle-Hansen H, Kurz M, Tobro H, Kaur K, Stankiewicz M, Carlsson M, Morsund Å, Idicula T, Aamodt AH, Lund C, Næss H, et al. Tenecteplase versus alteplase for management of acute ischaemic stroke (NOR-TEST): a phase 3, randomised, open-label, blinded endpoint trial. The Lancet Neurology. 2017;16(10):781–8. [PubMed: 28780236]

23. Nesheim M, Fredenburgh JC, Larsen GR. The dissociation constants and stoichiometries of the interactions of Lys-plasminogen and chloromethyl ketone derivatives of tissue plasminogen activator and the variant ΔFEIX with intact fibrin. Journal of Biological Chemistry. 1990;265(35):21541–8.

24. Sakharov D v., Nagelkerkel JF, Rijken DC. Rearrangements of the fibrin network and spatial distribution of fibrinolytic components during plasma clot lysis: Study with confocal microscopy. Journal of Biological Chemistry [Internet]. 1996;271(4):2133–8. Available from: 10.1074/jbc.271.4.2133

25. Longstaff C, Thelwell C, Williams SC, Silva MMCG, Szabó L, Kolev K. The interplay between tissue plasminogen activator domains and fibrin structures in the regulation of fibrinolysis: Kinetic and microscopic studies. Blood. 2011;117(2):661–8. [PubMed: 20966169]

26. Donnan GA, Davis SM, Parsons MW, Ma H, Dewey HM, Howells DW. How to make better use of thrombolytic therapy in acute ischemic stroke. Nature Reviews Neurology [Internet]. 2011;7(7):400–9. Available from: 10.1038/nrneurol.2011.89 [PubMed: 21670766]

27. Wang YF, Tsirka SE, Strickland S, Stieg PE, Soriano SG, Lipton SA. Tissue plasminogen activator (tPA) increase neuronal damage after focal cerebral ischemia in wild-type and tPA-deficient mice. Nature Medicine [Internet]. 1998;4(2):228–31. Available from: 10.1038/nm0298-228

28. Sakharov D v, Barrertt-Bergshoeff M, Hekkenberg RT, Rijken DC. Fibrin-specificity of a plasminogen activator affects the efficiency of fibrinolysis and responsiveness to ultrasound: comparison of nine plasminogen activators in vitro. Thrombosis and haemostasis. 1999 Apr;81(4):605–12. [PubMed: 10235448]

29. Horrevoets AJG, Pannekoek H, Nesheim ME. A steady-state template model that describes the kinetics of fibrin- stimulated [Glu1]- and [Lys78]plasminogen activation by native tissue- type plasminogen activator and variants that lack either the finger or kringle-2 domain. Journal of Biological Chemistry. 1997;272(4):2183–91.

30. de Vries C, Veerman H, Koornneef E, Pannekoek H. Tissue-type plasminogen activator and its substrate Glu-plasminogen share common binding sites in limited plasmin-digested fibrin. Journal of Biological Chemistry. 1990;265(23):13547–52.

31. Jung He Wu, Diamond SL. Tissue plasminogen activator (tPA) inhibits plasmin degradation of fibrin: A mechanism that slows tPA-mediated fibrinolysis but does not require α2- antiplasmin or leakage of intrinsic plasminogen. Journal of Clinical Investigation. 1995;95(6):2483–90.

32. Kim PY, Tieu LD, Stafford AR, Fredenburgh JC, Weitz JI. A high affinity interaction of plasminogen with fibrin is not essential for efficient activation by tissue-type plasminogen activator. Journal of Biological Chemistry. 2012;287(7):4652–61.

33. Onundarson PT, Francis CW, Marder VJ. Depletion of plasminogen in vitro or during thrombolytic therapy limits fibrinolytic potential. The Journal of laboratory and clinical medicine. 1992 Jul;120(1):120–8. [PubMed: 1613318]
34. Baeten KM, Richard MC, Kanse SM, Mutch NJ, Degen JL, Booth NA. Activation of single-chain urokinase-type plasminogen activator by platelet-associated plasminogen: A mechanism for stimulation of fibrinolysis by platelets. Journal of Thrombosis and Haemostasis. 2010;8(6):1313–22. [PubMed: 20180903]
35. Disharoon D, Marr DWM, Neeves KB. Engineered microparticles and nanoparticles for fibrinolysis. Journal of Thrombosis and Haemostasis. 2019;17(12):2004–15. [PubMed: 31529593]
36. Hu J, Huang W, Huang S, ZhuGe Q, Jin K, Zhao Y. Magnetically active Fe3O4 nanorods loaded with tissue plasminogen activator for enhanced thrombolysis. Nano Research. 2016;9(9):2652–61.
37. Huang L, ZhuGe Q, Cheng R, Zhao Y, Mao L, Yang B, Jin K, Huang W. Acceleration of Tissue Plasminogen Activator-Mediated Thrombolysis by Magnetically Powered Nanomotors. ACS Nano. 2014;8(8):7746–54. [PubMed: 25006696]
38. Voros E, Cho M, Ramirez M, Palange AL, de Rosa E, Key J, Garami Z, Lumsden AB, Decuzzi P. TPA Immobilization on Iron Oxide Nanocubes and Localized Magnetic Hyperthermia Accelerate Blood Clot Lysis. Advanced Functional Materials. 2015;25(11):1709–18.
39. Chen JP, Yang PC, Ma YH, Wu T. Characterization of chitosan magnetic nanoparticles for in situ delivery of tissue plasminogen activator. Carbohydrate Polymers [Internet]. 2011;84(1):364–72. Available from: 10.1016/j.carbpol.2010.11.052
40. Ma YH, Wu SY, Wu T, Chang YJ, Hua MY, Chen JP. Magnetically targeted thrombolysis with recombinant tissue plasminogen activator bound to polyacrylic acid-coated nanoparticles. Biomaterials [Internet]. 2009;30(19):3343–51. Available from: 10.1016/j.biomaterials.2009.02.034 [PubMed: 19299010]
41. Yang HW, Hua MY, Lin KJ, Wey SP, Tsai RY, Wu SY, Lu YC, Liu HL, Wu T, Ma YH. Bioconjugation of recombinant tissue plasminogen activator to magnetic nanocarriers for targeted thrombolysis. International Journal of Nanomedicine. 2012;7:5159–73. [PubMed: 23055728]
42. Han K, Shields CW, Velev OD. Engineering of Self-Propelling Microbots and Microdevices Powered by Magnetic and Electric Fields. Advanced Functional Materials. 2018;28(25):1–14.
43. Yang T, Tasci TO, Neeves KB, Wu N, Marr DWM. Magnetic Microlassos for Reversible Cargo Capture, Transport, and Release. Langmuir. 2017;33(23):5932–7. [PubMed: 28318267]
44. Yang T, Sprinkle B, Guo Y, Qian J, Hua D, Donev A, Marr DWM, Wu N. Reconfigurable microbots folded from simple colloidal chains. Proceedings of the National Academy of Sciences of the United States of America. 2020;117(31):18186–93. [PubMed: 32680965]
45. Ma F, Wang S, Wu DT, Wu N. Electric-field–induced assembly and propulsion of chiral colloidal clusters. Proceedings of the National Academy of Sciences [Internet]. 2015;112(20):6307–12. Available from: http://www.pnas.org/lookup/doi/10.1073/pnas.1502141112
46. Sen A, Ibele M, Hong Y, Velegol D. Chemo and phototactic nano/microbots. Faraday Discussions. 2009;143:9–14. [PubMed: 20334091]
47. Aghakhani A, Yasa O, Wrede P, Sitti M. Acoustically powered surface-slipping mobile microrobots. Proceedings of the National Academy of Sciences of the United States of America. 2020;117(7):3469–77. [PubMed: 32015114]
48. Chen XZ, Jang B, Ahmed D, Hu C, de Marco C, Hoop M, Mushtaq F, Nelson BJ, Pané S. Small-Scale Machines Driven by External Power Sources. Advanced Materials. 2018;30(15):1–22.
49. Challis LJ. Mechanisms for interaction between RF fields and biological tissue. Bioelectromagnetics. 2005;26(SUPPL. 7):98–106.
50. Martel S Presenting a New Paradigm in Cancer Therapy: Delivering therapeutic agents using navigable microcarriers. IEEE Pulse. 2014;5(3):48–55. [PubMed: 24838212]
51. Schmidt CK, Medina-Sánchez M, Edmondson RJ, Schmidt OG. Engineering microrobots for targeted cancer therapies from a medical perspective. Nature Communications [Internet]. 2020;11(1):1–18. Available from: 10.1038/s41467-020-19322-7
52. Ullrich F, Bergeles C, Pokki J, Ergeneman O, Erni S, Chatzipirpiridis G, Pané S, Framme C, Nelson BJ. Mobility experiments with microrobots for minimally invasive intraocular surgery. Investigative Ophthalmology and Visual Science. 2013;54(4):2853–63. [PubMed: 23518764]

53. Li J, Li X, Luo T, Wang R, Liu C, Chen S, Li D, Yue J, Cheng SH, Sun D. Development of a magnetic microrobot for carrying and delivering targeted cells. Science Robotics. 2018;3(19).
54. Tasci TO, Disharoon D, Schoeman RM, Rana K, Herson PS, Marr DWM, Neeves KB. Enhanced Fibrinolysis with Magnetically Powered Colloidal Microwheels. Small. 2017;1–11.
55. Deodhar G v., Adams ML, Joardar S, Joglekar M, Davidson M, Smith WC, Mettler M, Toler SA, Davies FK, Williams SKR, Trewyn BG. Conserved Activity of Reassociated Homotetrameric Protein Subunits Released from Mesoporous Silica Nanoparticles. Langmuir. 2018;34(1):228–33. [PubMed: 29231740]
56. Martin-Ortigosa S, Valenstein JS, Lin VSY, Trewyn BG, Wang K. Gold functionalized mesoporous silica nanoparticle mediated protein and DNA codelivery to plant cells via the biolistic method. Advanced Functional Materials. 2012;22(17):3576–82.
57. Martin-Ortigosa S, Peterson DJ, Valenstein JS, Lin VSY, Trewyn BG, Alexander Lyznik L, Wang K. Mesoporous silica nanoparticle-mediated intracellular cre protein delivery for maize genome editing via loxP site excision. Plant Physiology. 2014;164(2):537–47. [PubMed: 24376280]
58. Suteewong T, Sai H, Lee J, Bradbury M, Hyeon T, Gruner SM, Wiesner U. Ordered mesoporous silica nanoparticles with and without embedded iron oxide nanoparticles: Structure evolution during synthesis. Journal of Materials Chemistry. 2010;20(36):7807–14.
59. Barrett EP, Joyner LG, Halenda PP. The Determination of Pore Volume and Area Distributions in Porous Substances. I. Computations from Nitrogen Isotherms. Journal of the American Chemical Society. 1951;73(2):373–80.
60. Corricelli M, Depalo N, di Carlo E, Fanizza E, Laquintana V, Denora N, Agostiano A, Striccoli M, Curri ML. Biotin-decorated silica coated PbS nanocrystals emitting in the second biological near infrared window for bioimaging. Royal Society of Chemistry. 2013;00(1–3):1–10.
61. Tasci TO, Herson PS, Neeves KB, Marr DWM. Surface-enabled propulsion and control of colloidal microwheels. Nature Communications [Internet]. 2016;7:10225. Available from: http://www.nature.com/doifinder/10.1038/ncomms10225
62. Rijken DC, Sakharov D v. Basic principles in thrombolysis: Regulatory role of plasminogen. Thrombosis Research. 2001;103(SUPPL. 1):41–9.
63. Bannish BE, Keener JP, Fogelson AL. Modelling fibrinolysis: A 3D stochastic multiscale model. Mathematical Medicine and Biology. 2014;31(1):17–44. [PubMed: 23220403]
64. Torno MD, Kaminski MD, Xie Y, Meyers RE, Mertz CJ, Liu X, O'Brien WD, Rosengart AJ. Improvement of in vitro thrombolysis employing magnetically-guided microspheres. Thrombosis Research. 2008;121(6):799–811. [PubMed: 17942144]

Essentials:

- The speed of fibrinolysis is limited by kinetic and transport barriers
- Plasminogen depletion is rate limiting at high tissue plasminogen activator (tPA) concentrations
- Magnetically powered microwheels were designed to co-deliver tPA and plasminogen
- Microwheel mediated fibrinolysis exceeds the biochemical speed limit

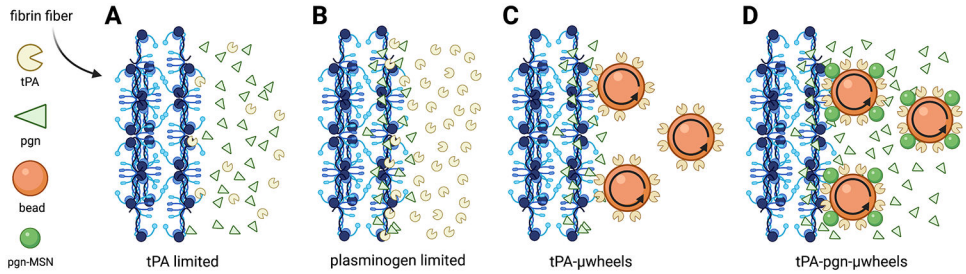

Fig. 1:

A) The rate-limiting steps of fibrinolysis include the transport to a clot and binding of tPA to fibrin fibers at low tPA concentrations. B) At sufficiently high tPA concentrations, its substrate plasminogen (pgn), becomes the limiting factor in fibrinolysis. C) These rate-limiting steps are overcome using magnetically powered μwheels, superparamagentic beads (orange spheres) that self-assemble in rotating magnetic fields. When μwheeels are coupled to tPA (tPA-μwheels) they accumulate at the clot interface leading to high tPA concentrations and plasminogen limited fibrinolysis. D) By attaching plasminogen releasing nanoparticles (green spheres) to μwheels (tPA-pgn-μwheels) co-delivery of both enzyme and substrate are achieved yielding fibrinolysis rates that overcomes plasminogen-limited fibrinolysis.

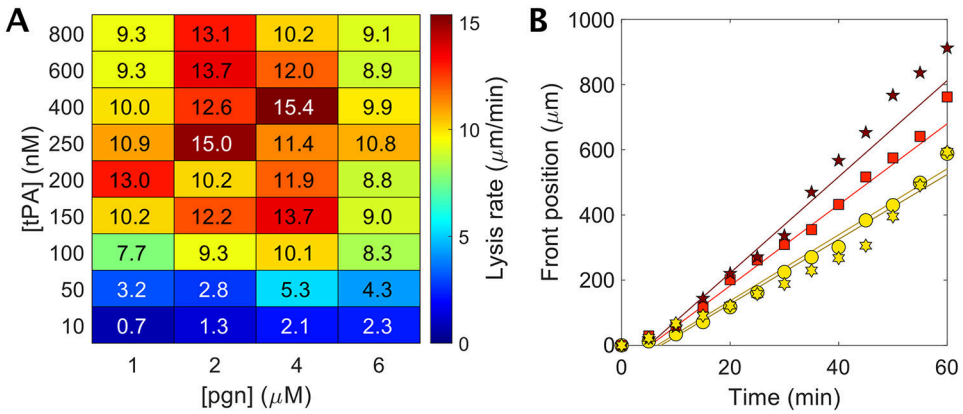

Fig. 2:

Measuring the fibrinolytic speed limit of plasma clots. A) Heat map of lysis rates as a function of tPA and plasminogen (pgn) concentrations. The accelerated fibrinolysis (AF) zone incorporates regions with lysis greater than 13.5 μm/min. Symbols denote data shown in panel B. Overlaid numbers indicate exact lysis rates measured. The numbers align with the exact concentrations of tPA and plasminogen used for that measurement. n = 1 – 3. Lysis rates are average rates over 60 min (Fig. 2B). B) Dissolution of fibrin at 400 nM tPA with endogeneous plasma plasminogen concentration (1 μM) and the addition of exogenous plasminogen up to 6 μM total plasminogen concentration. Lysis rates are linear with time. Regression fits for 1, 2, 4 and 6 μM data have R^2 = 0.95, 0.98, 0.98, and 0.95, respectively.

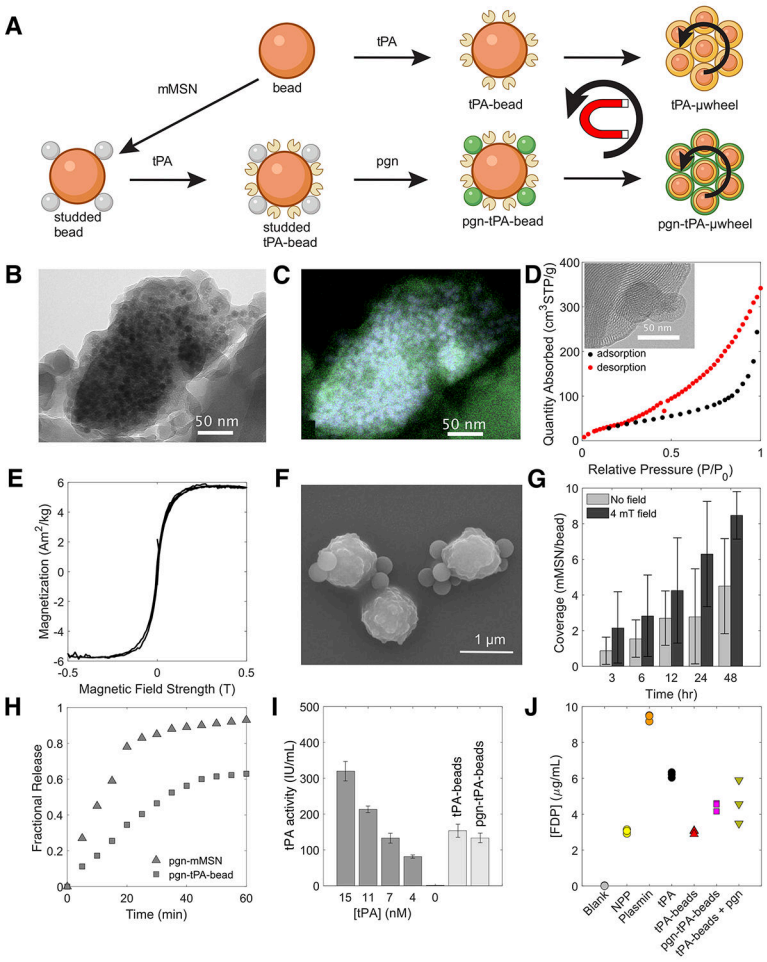

Fig. 3:

Synthesis and characterization of magnetic mesoporous silica nanoparticles (mMSN) and their coupling to superparamagnetic beads. A) Schematic of tPA-functionalization, mMSN-bead coupling, and plasminogen (pgn) loading to create tPA- and tPA-pgn-μwheels. B) Transmission electron microraph (TEM) of mMSN. Darker areas are Fe3O4 domains incorporated into the silica matrix. C) High-angle annular dark field energy-dispersive X-ray (HAADF-EDS) spectrum showing iron oxide domains (blue) distributed throughout silica matrix (green). D) Representative BJH isotherm data with TEM image of pore structure (inset). E) Magnetization profile for mMSN. F) Scanning electron micrograph (SEM) of studded beads. G) Coverage of mMSN to beads as a function of mixing time in the with and without a 4 mT magnetic field. H) Plasminogen release profile for pgn-mMSN and pgn-tPA-beads at a number density of $10^6/\mu L$. Fractional release is normalized to the total plasminogen loading as measured by spectrometry. I) Activity of 10^5/μL bead populations compared to solvated tPA, measured using a fluorogenic substrate. J) Concentration of FDP in NPP after 60 min incubation with bead populations having an equivalent activity to 50 nM tPA.

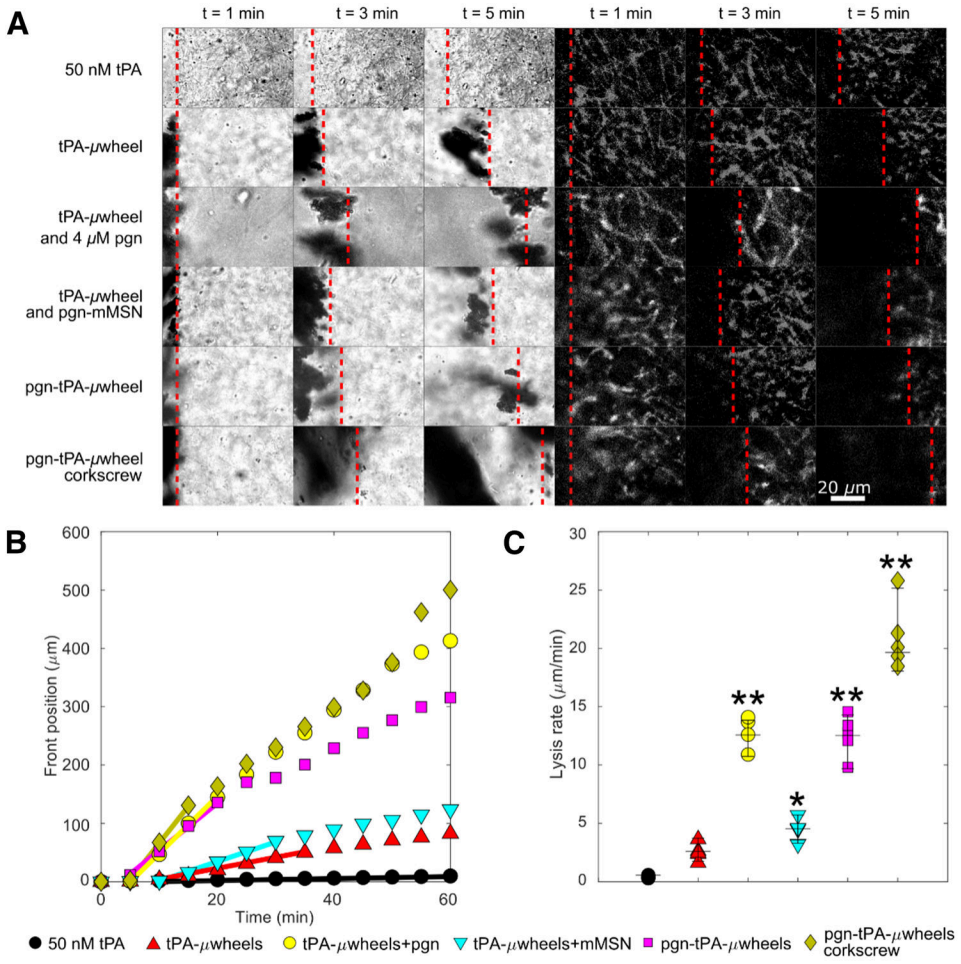

Fig. 4:

A) Time lapse of lysis of plasma clots using different μwheel formulations. Brightfield at left, and fluorescently labeled fibrin(ogen) at right. Dashed lines indicate the front position. B) FDP generated by each formulation. C) Representative lysis curves for each formulation. Lines indicate periods of maximum lysis rates lasting for a minimum of 10 min. D) Maximum lysis rates for each formulation. Corkscrew condition uses pgn-tPA-μwheels. Dotted line indicates biochemical speed limit (see Fig. 2B). *Statistically significant from 50 nM tPA with p-value 0f 0.01. **Statistically significant from 50 nM tPA with p-values <0.0001.